UCRL-PROC-202259

LAWRENCE
LIVERMORE
NATIONAL
LABORATORY

Crystal level simulations using Eulerian finite element methods

N.R. Barton, D.J. Benson and R. Becker

June 13, 2004

NUMIFORM 2004: The 8th International Conference on
Numerical Methods in Industrial Forming Processes,
The Ohio State University, Columbus, Ohio, USA
June 13-17, 2004

Disclaimer

This document was prepared as an account of work sponsored by an agency of the United States Government. Neither the United States Government nor the University of California nor any of their employees, makes any warranty, express or implied, or assumes any legal liability or responsibility for the accuracy, completeness, or usefulness of any information, apparatus, product, or process disclosed, or represents that its use would not infringe privately owned rights. Reference herein to any specific commercial product, process, or service by trade name, trademark, manufacturer, or otherwise, does not necessarily constitute or imply its endorsement, recommendation, or favoring by the United States Government or the University of California. The views and opinions of authors expressed herein do not necessarily state or reflect those of the United States Government or the University of California, and shall not be used for advertising or product endorsement purposes.

This work was performed under the auspices of the U.S. Department of Energy by University of California, Lawrence Livermore National Laboratory under Contract W-7405-Eng-48.

Crystal level simulations using Eulerian finite element methods

Nathan R. Barton*, David J. Benson* and Richard Becker†

* *University of California, San Diego; Department of Mechanical and Aerospace Engineering; 9500 Gilman Dr; La Jolla, CA 92093-0411*
† *Lawrence Livermore National Laboratory; P.O. Box 808, L-228; Livermore, CA 94551*

Abstract.
Over the last several years, significant progress has been made in the use of crystal level material models in simulations of forming operations. However, in Lagrangian finite element approaches simulation capabilities are limited in many cases by mesh distortion associated with deformation heterogeneity. Contexts in which such large distortions arise include: bulk deformation to strains approaching or exceeding unity, especially in highly anisotropic or multiphase materials; shear band formation and intersection of shear bands; and indentation with sharp indenters. Investigators have in the past used Eulerian finite element methods with material response determined from crystal aggregates to study steady state forming processes. However, Eulerian and Arbitrary Lagrangian-Eulerian (ALE) finite element methods have not been widely utilized for simulation of transient deformation processes at the crystal level. The advection schemes used in Eulerian and ALE codes control mesh distortion and allow for simulation of much larger total deformations. We will discuss material state representation issues related to advection and will present results from ALE simulations.

INTRODUCTION

In the context of crystal scale continuum models of material behavior, localization and deformation heterogeneity, while often of interest, pose substantial hurdles to simulation efforts. This is particularly true for multiphase materials and for materials with large anisotropy at the crystal level [1, 2, 3]. But deformation heterogeneity also poses difficulties for simulations of relatively isotropic single phase materials, especially when large macroscopic strains are of interest.

Three dimensional remeshing provides one possible remedy. However, general remeshing is challenging in the face of domains with internal material boundaries and a detailed representation of the material state. Eulerian finite element methods offer another route by which problems with heterogeneous deformation may be tackled. These methods may be viewed as performing continuous remeshing, with well developed capabilities for tracking material boundaries. Progress on advection schemes and boundary determination methods has been sufficient to allow for simulations of problems in micromechanics [4, 5, 6]. Issues do remain related to the advection of lattice orientation and other tensorial state variable descriptors, and these issues are partially addressed in the work presented here.

A crystal level material model is developed and implemented in an Eulerian finite element framework. The model allows for elastic and thermal lattice distortion and for restricted slip crystal plasticity. While it is in many situations appropriate to specialize models to small elastic strains, as is done in [7], Eulerian finite element programs are often used to simulate dynamic loading conditions. Such loading conditions can produce large pressures and thus large lattice strains. For this reason, we employ a logarithmic lattice strain measure and allow bulk deformation of the lattice to be large.

Example simulations are conducted to demonstrate the model capabilities under quasi-static and dynamic conditions. The quasi-static simulations are conducted for channel die compression of a single crystal of metastable orientation, corresponding to the work reported in [8] and [9]. The material is compressed to a 90% reduction in height and, due to initial small perturbations in the lattice orientation, the crystal lattice orientation breaks up into alternating layers of the two 'copper' texture components. Results are compared to experimental findings and Lagrangian simulation results reported in [8]. Dynamic simulations of shock induced void collapse serve to demonstrate the large pressure capabilities of the model.

CRYSTAL LEVEL MATERIAL MODEL

In many regards the material model is similar to existing models for deformation of elasto-viscoplastic crystals [10, 7]. However, in contrast to many other models, both elastic and thermal deformation of the lattice are combined into a single lattice stretch in the multiplicative decomposition of the deformation gradient. Another key difference is that the state variables are stored in a form amenable to advection. As the model is similar to others existing in the literature, we outline its features and implementation below but do not discuss it in detail.

Multiplicative decomposition of the deformation gradient takes the form

$$\mathbf{F} = \mathbf{V} \cdot \mathbf{R} \cdot \mathbf{F}^{\mathrm{p}} \tag{1}$$

where $\mathbf{V}$ is symmetric and embodies both elastic and thermal lattice straining; $\mathbf{R}$ is the lattice rotation; and $\mathbf{F}^{\mathrm{p}}$ is deformation due to dislocation glide. We then have

$$\mathbf{L} = \dot{\mathbf{F}} \cdot \mathbf{F}^{-1} = \dot{\mathbf{V}} \cdot \mathbf{V}^{-1} + \mathbf{V} \cdot \hat{\mathbf{L}} \cdot \mathbf{V}^{-1} \tag{2}$$

$$\hat{\mathbf{L}} = \dot{\mathbf{R}} \cdot \mathbf{R}^{\mathrm{T}} + \mathbf{R} \cdot \bar{\mathbf{L}} \cdot \mathbf{R}^{\mathrm{T}} \quad , \quad \bar{\mathbf{L}} = \sum_{\alpha=1}^{n} \dot{\gamma}^{\alpha} (\bar{\mathbf{s}}^{\alpha} \otimes \bar{\mathbf{m}}^{\alpha}) \tag{3}$$

with Equation (3) including the standard restricted slip assumption for the kinematics of crystal plasticity.

Due to its advantageous properties in decoupling bulk and distortional deformation, a logarithmic form is used for the lattice strain measure: $\hat{\mathbf{E}} = \ln(\mathbf{V})$. The relation

$$\hat{\tau} = f_{\mathscr{L}}(\hat{\mathbf{E}}, e) \tag{4}$$

governs the elastic response, with $\hat{\tau} = \hat{J}\sigma$ and $\hat{J} = \det(\mathbf{V})$. In this relation, temperature could be substituted for the internal energy e.

For metals of cubic symmetry, it is typically acceptable to assume that the distortional lattice strains are small even when the bulk strains are large. Together with the use of the logarithmic lattice strain measure, this fact allows for substantial simplification of the model.[1] First define $a = (\det(\mathbf{V}))^{1/3}$ such that $\mathbf{V} = a\mathbf{V}^*$ and $\det(\mathbf{V}^*) = 1$. Then

$$\ln(\mathbf{V}) = \ln(a)\mathbf{I} + \ln(\mathbf{V}^*) \tag{5}$$

and we have $\mathrm{tr}(\ln(\mathbf{V}^*)) = \ln(\det(\mathbf{V}^*)) = 0$ so that $\mathrm{tr}(\ln(\mathbf{V})) = \ln(\det(\mathbf{V}))$ as expected.

$\hat{\mathbf{E}}'$ is directly related to the deviatoric part of the stress and the stress is restricted in magnitude by plastic deformation mechanisms. Therefore, it is safe to assume that $\hat{\mathbf{E}}' = \ln(\mathbf{V}^*)$ is always small. Defining $\mathbf{V}^* = \mathbf{I} + \varepsilon^*$, ε^* too is always small and $\ln(\mathbf{V}^*)$ is approximately equal to ε^*. As $\mathrm{tr}(\ln(\mathbf{V}^*)) = 0$, $\mathrm{tr}(\varepsilon^*)$ is approximated as zero. Decomposing $\mathbf{V}$ according to

$$\mathbf{V} = \mathbf{I} + \varepsilon = a(\mathbf{I} + \varepsilon^*) \tag{6}$$

we have $\varepsilon^* = \varepsilon^{*\prime} = \frac{1}{a}\varepsilon'$. All together, the lattice strain measure is approximated by

$$\hat{\mathbf{E}}' = \frac{1}{a}\varepsilon' \quad , \quad \mathrm{tr}(\hat{\mathbf{E}}) = \ln(\det(\mathbf{V})). \tag{7}$$

As a further approximation related to the lattice stretch, we use

$$\mathbf{V}^{-1} = \frac{1}{a}(\mathbf{I} - \varepsilon^*). \tag{8}$$

The trace of $\hat{\mathbf{E}}$ depends directly on the determinant of $\mathbf{V}$ and no approximations are used calculating $\mathrm{tr}(\hat{\mathbf{E}})$.

Using the equivalence between internal and external work rates, the resolved stress on a slip system α is found to be, under the small deviatoric lattice strain assumption,

$$\tau^{\alpha} = \hat{\tau} : (\hat{\mathbf{s}}^{\alpha} \otimes \hat{\mathbf{m}}^{\alpha}). \tag{9}$$

The small deviatoric lattice strain assumption also allows for appreciable simplification of the calculations. This is particularly true when components of the lattice strain and its rate are computed in a frame that rotates with the lattice. Details of the calculations, including the time integration scheme and material tangent stiffness calculation, are omitted for space reasons.

As a final note on the material model, the logarithmic lattice strain measure allows for the use of a variety of equations of state for the pressure-volume-temperature relationship. In the shock loading results presented below, a Grüneisen equation of state is used.

ADVECTION OF CRYSTAL LEVEL STATE VARIABLES

The simulations discussed below are conducted in Raven, a multi-material two dimensional arbitrary Lagrangian-Eulerian (ALE) finite element program. Raven makes use of an 'operator split' method for the Lagrangian and Eulerian steps of the calculation. During the Lagrangian step, the mesh follows material and becomes distorted. In the Eulerian or 'advection' step, the solution on the distorted mesh is mapped to the new mesh. This new mesh may either be the original undistorted mesh or a mesh which follows a general motion.

During advection, a given state variable value in an element becomes a weighted average of the value in that element and its neighbors. The weights depend on the velocity field around the element and on the type of advection scheme. Raven uses the van Leer MUSCL algorithm [11] for material transport (advection). Details of

[1] A fully large strain version of the model has been implemented and tested, but due to space considerations we do not include results here.

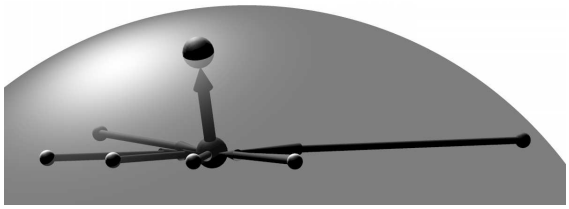

FIGURE 1. Normalized quaternion averaging procedure.

advection schemes are not described here – the interested reader is referred to the comprehensive review paper by Benson [12]. The Lagrangian part of the program follows the standard formulation used in many Eulerian finite element programs and makes use of reduced integration with hourglass control.

If the advection scheme is to return meaningful results for the post-advection state variables, the variables must be stored in such a way that weighted averages are meaningful. For scalar state variables, such as an average dislocation density, no special precautions need to be taken. However, the lattice strain and the lattice orientation are tensorial and require more care.

First consider the lattice orientation, represented as the rotation relating a fixed coordinate frame and the lattice frame – that is as an element of SO(3). The lattice orientation may be parameterized using quaternions, which are the numbers

$$Q = \{q_0; \mathbf{q}\} \quad \text{with} \quad \mathbf{q} = \{q_1\, q_2\, q_3\}. \tag{10}$$

A quaternion with unit norm is called normalized:

$$\|Q\|^2 = q_0^2 + \|\mathbf{q}\|^2 = 1 \tag{11}$$

and normalized quaternions reside on the unit 4-sphere, H_4. To parameterize SO(3), let $\mathbf{x} = \{q_0\, q_1\, q_2\, q_3\} \in H_4$ and identify antipodes ($+\mathbf{x}$ and $-\mathbf{x}$). Metrical properties of the parameter space are such that a meaningful weighted average of orientations is obtained from

$$\mathbf{m} = \frac{\bar{\mathbf{x}}}{\|\bar{\mathbf{x}}\|} \quad \text{where} \quad \bar{\mathbf{x}} = \sum_i w^{(i)} \mathbf{x}^{(i)} \tag{12}$$

with weights $w^{(i)}$. Figure 1 contains a graphical representation of this process, reduced to the 3-sphere for visualization purposes. Because antipodes on H_4 parameterize the same orientation, some care must be taken in storing the parameters for advection. Assuming the lattice orientation does not change by a large angular amount over a time step, the sign of the normalized quaternion is chosen to be the one giving closest alignment to the beginning of step normalized quaternion. While both antipodes are acceptable parameterizations, the averaging that occurs during advection is meaningful only for quaternions that are clustered on H_4. For further details related to average orientations using quaternions, see [13, 14]. The book by Altmann [15] contains a more general discussion of quaternions.

Sharp jumps in lattice orientation may occur at grain boundaries, and averaging over such boundaries is undesirable. Averaging lattice orientation across a phase boundary is meaningless. These situations are avoided in multi-material Eulerian finite element codes, such as Raven, through the introduction of material boundaries. Such boundaries allow for distinct regions of material and the state in these distinct regions does not mix during advection.

The remaining tensorial state variable describes the stretch of the crystal lattice. It is intimately associated with changes in lattice plane spacing and thus it is tied to the orientation of the lattice itself. We therefore store the components of the strain in the lattice frame for advection. In order to reduce round-off errors, it is actually the components of $\varepsilon = \mathbf{V} - \mathbf{I}$ which are advected. If there were other tensorial state variables tied to the lattice, such as a tensor describing some feature of the dislocation density, we would store their components in the lattice frame as well.

CHANNEL DIE COMPRESSION SIMULATIONS

As an example application of the crystal level material model in an ALE finite element code, we consider channel die compression of an aluminum single crystal to a height reduction of 90%. This corresponds to a true strain of roughly -2.3. In analogy to rolling, the extension direction will be called the rolling directly (RD), the compression direction will be called the normal direction (ND), and the constrained direction will be called the transverse direction (TD). As in [8], the nominal initial lattice orientation is chosen so that a $\langle 100 \rangle$ crystal direction is aligned with ND and a $\langle 01\bar{1} \rangle$ direction is aligned with RD. From the experimental results in [8], we know that high angle misorientation boundaries tend to develop with their normals aligned with ND, providing some justification for plane strain simulations of the deformation.

In the Lagrangian finite element simulations in [8], elements are badly distorted by a strain of -1.2, leading to inaccuracies in the solution quantities. In contrast, we are able, with Raven, to simulate the full strain history without adverse effects from element distortion. As the experiments in [8] were performed under quasi-static conditions, the simulations in Raven neglect inertial terms. At the finite element level, an implicit solver is used, and the tangent stiffness matrices from the material model are used in forming the finite element stiffness matrices.

The deformation is restricted to the RD-ND plane and on both ND-normal mesh faces we apply mirror boundary conditions. On the left RD-normal face we apply a mirror boundary condition and the right RD-normal mesh face is traction free. The mesh remains regular throughout the deformation, and follows the deformation in an average sense. Along the right RD-normal mesh face, material may flow in and out of the mesh due to heterogeneities in the deformation. The state of material flowing into the mesh is obtained by extrapolation. The mesh is composed of 160 elements along RD by 40 elements along ND.

Note that while the deformation is restricted to a plane, the model described above and its implementation are fully three dimensional. Plastic deformation occurs by slip on the twelve standard $\{111\}\langle 110\rangle$ slip systems for face centered cubic crystals.

The nominal initial lattice orientation is metastable under the applied deformation mode. When perturbed away from the nominal orientation, the crystal's lattice will rotate toward one of two stable texture components as the material deforms. In order to begin this process, we perturb the lattice orientation in each finite element by a random amount of magnitude less than 0.2° about the TD axis. As in [8], we also conduct simulations for perturbations about an initial orientation which is rotated by 3.5° about the compression axis (ND). This corresponds more accurately to the actual starting lattice orientation for the experiments in [8]. In this case, the redundant slip system activity required to achieve a net in-plane deformation mode slows the rate of lattice reorientation.

As the material deforms, the lattice orientations tend toward one of two 'copper' type texture components. These two components are apparent in Figure 2, which shows the orientation distribution function (ODF).

Misalignment of the nominal initial orientation by 3.5° is enough to produce noticeable differences in lattice reorientation rates. These differences are apparent in Figure 3, which shows the peak pole figure intensity and its orientation for the aligned and misoriented conditions.

At the beginning of the simulations, a reduction in peak intensity indicates a spreading in the texture components and the development of transition regions between the peaks in the ODF. As the deformation continues, the lattice orientations begin to collect at the stable texture components, and the pole figure peak intensity increases again. Lattice reorientation rates are slower in the misoriented case, due to increased redundant slip system activity, and intermediate lattice orientations are not eliminated as quickly.

Without any constraints on the in-plane shear in the crystals, the stable lattice reorientation is 35.26° (vertical axis in Figure 3(b)). Mutual constraint among the regions of material slows the approach of the lattice orientation to this ideal value. Peak pole figure location results in

FIGURE 2. Isosurface ODF plot in Rodrigues space, with isosurfaces at 100 and 300 multiples of a uniform distribution (MUD); for aligned nominal initial lattice orientation; at a strain of -2.3.

Figure 3(b) indicate that lattice reorientation rates are under-predicted, especially in the higher strain range.

A likely cause of the under-prediction of lattice reorientation rates is the mixing of lattice orientation from the two stable components during to advection. The implicit formulation in Raven uses reduced integration with hourglass control, allowing some spurious fluctuations in the velocity field and thus extra mixing of state variable quantities. Lagrangian finite element results reported in Figure 18 of [8] achieve better agreement with experimental lattice reorientation rates out to the maximum simulated true strain of -1.2.

VOID COLLAPSE SIMULATIONS

As a second example application, we consider shock induced void collapse in copper. These simulation are conducted at a relatively low shock pressure of 1.4 GPa so that pressure effects do not completely dominate material strength effects. The two-dimensional simulations are of single crystals with a cylindrical void initially one micron in diameter. Three different crystal orientations give shocks running along [100], [110], and [111] directions. We report briefly on the variations in the response for these three different crystal orientations. We use the MTS model for the slip system kinetics [17], and a dislocation density model for the material hardening. Parameters are either taken directly from [17] or chosen to fit the experimental data reported in [17].

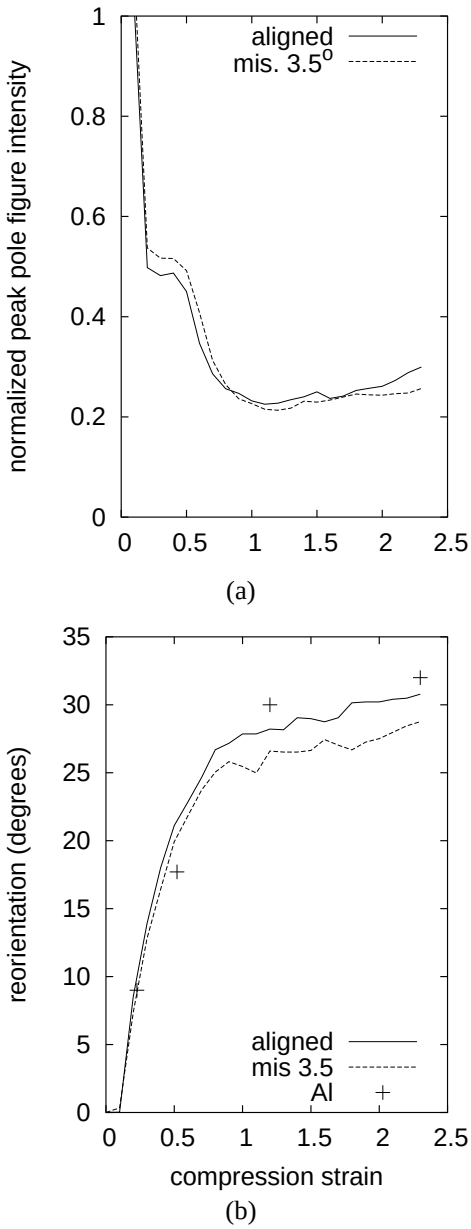

FIGURE 3. Evolution of (a) peak pole figure intensity and (b) typical pole reorientation angle, with aluminum [8] data.

While the effective strain in the bulk of the material is small, effective strains near the collapsed void are well in excess of unity. The large strains and high strain rates produced as the voids collapse drive up the dislocation density. Figure 4 shows the dislocation density in the region of the collapsed void. The shock has traveled from left to right. In the [100] shock direction case, the void has not completely collapsed. This is also the case in which the overall dislocation density increase is smallest.

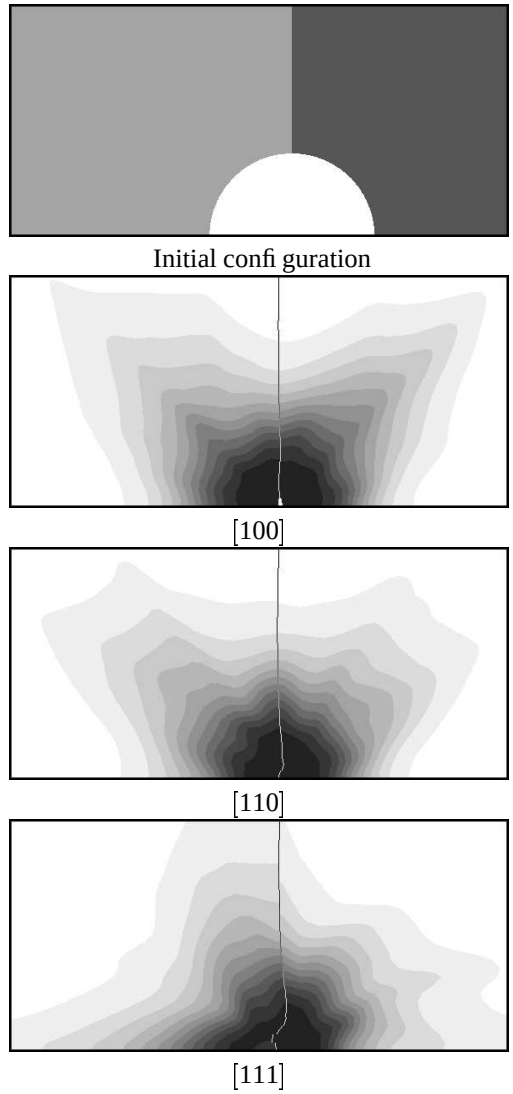

FIGURE 4. Total dislocation density near collapsed voids. The range is 10^7 (light) to $10^{11}\,\mathrm{cm}^{-2}$ (dark). Initial void diameter is 1 micron and the whole simulation domain is 5 by 5 microns – only part of the domain is shown in the above plots. The shocks traveled from left to right.

The contrasting lines in Figure 4 indicate the boundary between material on the upstream and downstream sides of the voids (that is between the two regions indicated in the initial configuration shown in the figure). In the [111] shock direction case, the shape of the void is unstable during collapse, resulting in undulation of the contrast line.

Higher shock pressures can result in jetting and local melting when the void collapses, but melting did not occur in the simulation results reported here. Peak temperatures for the [100], [110], and [111] shock directions are 648 K, 982 K, and 1016K respectively.

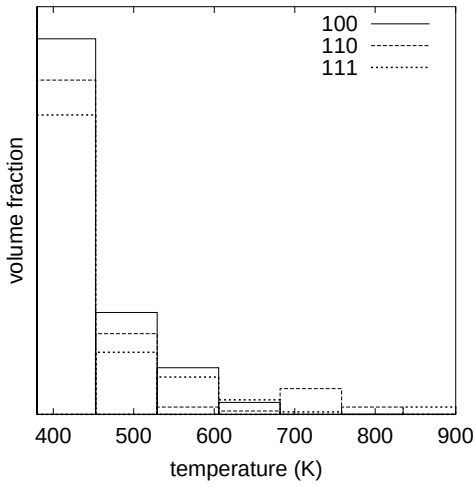

FIGURE 5. Residual temperature histograms.

Figure 5 contains histograms which more clearly indicate variations in residual temperature as a function of shock direction. To emphasize the effect of the void, the histogram bin containing the lowest temperature range, representative of the bulk temperature, has been left out of Figure 5. Overall, the [100] shock direction simulation shows the least heating.

DISCUSSION AND CONCLUSIONS

The model and its implementation in an Eulerian finite element context show promise. Results from the channel die compression simulations do not compare as well to experiments as one might hope. But efforts are under way to implement a new integration and state storage scheme that will eliminate the need for hourglass control.

With its large pressure capabilities and suitable state variable storage scheme, the model presented here may be used to simulate dynamic loading scenarios at the crystal level. Using the model, dynamic void growth and collapse may be investigated at the crystal level. Possible applications of the model range from dislocation generation kinetics in shocks to hot spot formation in energetic materials.

One can imagine many other simulation scenarios in which the above model might be used to investigate problems which are difficult to tackle using Lagrangian finite element methods. For example, indentation experiments can involve large localized deformations and might be simulated using a crystal model coupled with an Eulerian finite element program. Shear band formation, particularly with intersecting shear bands, might also be studied. In a Lagrangian finite element code, the mesh is potentially so distorted by the first band that a second band has great difficulty forming. Eulerian finite element programs, together with crystal level constitutive models and well chosen state variable storage schemes, are likely to see increasing use in simulations of deformations in micromechanics.

ACKNOWLEDGMENTS

This work was performed under the auspices of the U.S. Department of Energy by University of California Lawrence Livermore National Laboratory under contract No. W-7405-Eng-48.

REFERENCES

1. Steinkopff, T., and Sautter, M., *Modelling Simul. Mater. Sci. Eng.*, **5**, 1–21 (1997).
2. Barton, N. R., and Dawson, P. R., *Modelling Simul. Mater. Sci. Eng.*, **9**, 433–463 (2001).
3. Barton, N. R., and Dawson, P. R., *International Journal of Forming Processes*, **5**, 189–201 (2002).
4. Benson, D. J., *Compt. Methods Appl. Mech. & Eng.*, **151**, 343–360 (1998).
5. Fu, H.-H., Benson, D. J., and Meyers, M. A., *Acta Mater.*, **49**, 2567–2582 (2001).
6. Benson, D. J., *Appl. Mech. Rev.*, **55**, 151–165 (2002).
7. Marin, E. B., and Dawson, P. R., *Compt. Methods Appl. Mech. & Eng.*, **165**, 1–21 (1998).
8. Becker, R., Butler, J. F., Hu, H., and Lalli, L. A., *Met. Trans. A*, **22**, 45–58 (1991).
9. Liu, Q., Maurice, C., Driver, J., and Hansen, N., *Metall. Mater. Trans. A*, **29A**, 2333–2344 (1998).
10. McHugh, P. E., Asaro, R. J., and Shih, C. F., "Crystal plasticity models," in *Fundamentals of Metal-Matrix Composites*, edited by S. Suresh, A. Mortensen, and A. Needleman, Butterworth-Heinemann, 1993, chap. 8.
11. van Leer, B., *J. Comput. Phys.*, **23**, 276–299 (1977).
12. Benson, D. J., *Compt. Methods Appl. Mech. & Eng.*, **99**, 235–394 (1992).
13. Krieger Lassen, N. C., Juul Jensen, D., and Conradsen, K., *Acta Cryst.*, **A50**, 741–748 (1994).
14. Prentice, M. J., *J. R. Stat. Soc. B*, **48**, 214–222 (1986).
15. Altmann, S. L., *Rotations, Quaternions, and Double Groups*, Oxford University Press, 1986.
16. Köhlhoff, G. D., Hirsch, J., Schlippenbach, U. V., and Lücke, K., "Microstructure and recrystallization of rolled FCC-single crystals," in *The Sixth International Conference on Textures of Materials (ICOTOM6)*, Iron and Steel Institute of Japan, Tokyo, 1981, pp. 489–498.
17. Follansbee, P. S., and Kocks, U. F., *Acta Metall.*, **36**, 81–93 (1988).